JACS
JOURNAL OF THE AMERICAN CHEMICAL SOCIETY

ARTICLE

pubs.acs.org/JACS

Supramolecular Engineering of Intrinsic and Extrinsic Porosity in Covalent Organic Cages

Michael J. Bojdys, Michael E. Briggs, James T. A. Jones, Dave J. Adams, Samantha Y. Chong, Marc Schmidtmann, and Andrew I. Cooper*

Department of Chemistry and Centre for Materials Discovery, University of Liverpool, Crown Street, Liverpool L69 7ZD, U.K.

Supporting Information

ABSTRACT: Control over pore size, shape, and connectivity in synthetic porous materials is important in applications such as separation, storage, and catalysis. Crystalline organic cage molecules can exhibit permanent porosity, but there are few synthetic methods to control the crystal packing and hence the pore connectivity. Typically, porosity is either 'intrinsic' (within the molecules) or 'extrinsic' (between the molecules)—but not both. We report a supramolecular approach to the assembly of porous organic cages which involves bulky directing groups that frustrate the crystal packing. This generates, in a synthetically designed fashion, additional 'extrinsic' porosity between the intrinsically porous cage units. One of the molecular crystals exhibits an apparent Brunauer–Emmett–Teller surface area of 854 $m^2 g^{-1}$, which is higher than that of unfunctionalized cages of the same dimensions. Moreover, connectivity between pores, and hence guest uptakes, can be modulated by the introduction of halogen bonding motifs in the cage modules. This suggests a broader approach to the supramolecular engineering of porosity in molecular organic crystals.

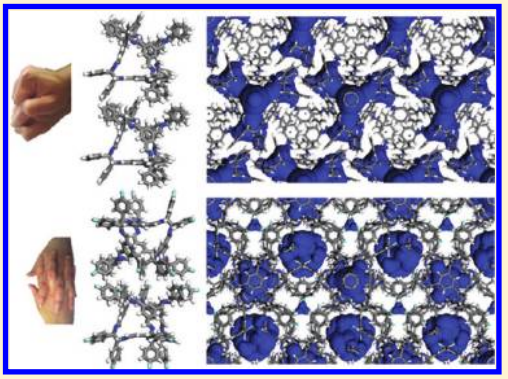

INTRODUCTION

Microporous materials—that is, materials with pores smaller than 2 nm—have generated much recent interest.[1−5] Recently, porous solids of entirely organic composition have extended the range of possible properties and applications. Microporous and mesoporous organic polymers[6−11] and covalent organic frameworks (COFs),[12,13] in particular, have scope for targeted applications because their constituent building blocks can be readily diversified using organic synthesis.[14] The surface area in such networks is generated typically via templating or scaffolding approaches;[15−18] as such, the porosity is a consequence of the solid state packing of the building blocks and is 'extrinsic' in nature. Other organic materials can exhibit 'intrinsic' porosity that results from the shape of the isolated molecular building blocks themselves, for example in the form of synthetically prefabricated pores, cavities, or windows. Examples of such 'porous molecules,'[19,20] include calixarenes[21,22] and a range of other small organic molecules with shape-persistent covalent cavities.[23−25]

Cage-like molecules are appealing as porous solids.[27−29] Recently, a family of porous organic cage compounds has been shown to demonstrate either extrinsic or intrinsic porosity, depending on the packing mode of the cages.[30−34] The cavities and windows in these molecules are created by a reversible [4 + 6] Schiff-base condensation[29,35] of amine and aldehyde components. Notably, packing of these cages—and hence the porosity of the resulting crystalline solids—is influenced by the bulkiness of the cage vertices.[30] The materials have permanent micropore structures and exhibit Brunauer–Emmett–Teller surface areas (SA_{BET}) of up to 624 $m^2 g^{-1}$ for smaller cages[30] and >1300 $m^2 g^{-1}$ for a larger [4 + 6] imine cage.[32,33] In principle, intrinsically porous organic cages may have advantages over networks and frameworks because they are solution processable and can be combined in a modular fashion to generate porous cocrystals comprising more than one molecular building block.[33]

In general, porous molecular crystals may be expected to have greater scope for structural rearrangement and polymorphism than crystalline porous frameworks, such as zeolites, MOFs, and COFs. This is because molecular organic crystals are assembled via weaker and less directional noncovalent forces in comparison with covalent and coordination frameworks. This can be an advantage or a disadvantage, depending on the context. For example, we have exploited the 'soft'[5] nature of porous molecular crystals in the preparation of materials with 'on/off' porosity switching behavior.[31] Such structural flexibility, however, might also prove undesirable in other cases and lead to irreversible loss of porosity. Moreover, even with the prospect of methods for predicting molecular crystal structures,[33,36] the modular and predictable assembly of multicomponent porous organic crystals assembled via noncovalent forces remains a major challenge. Hence, to achieve programmed assembly in porous molecular crystals, as demonstrated in isoreticular MOFs,[37] it is desirable to use the established tools of crystal engineering and supramolecular chemistry to direct molecular assembly.[38] For example,

Received: July 1, 2011
Published: September 07, 2011

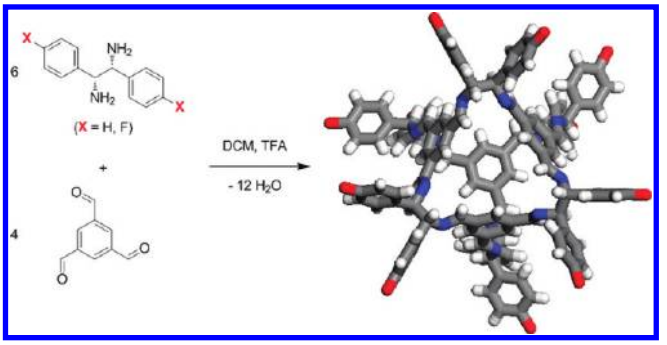

Figure 1. Reaction scheme for the [4 + 6] Schiff-base condensation yielding **CC9** (X = H) and **CC10** (X = F) cage molecules, as shown facing one of the triangular pore windows. C, N, and H atoms are colored gray, blue and white, respectively.

to generate additional porosity it may be necessary to engineer both intrinsic *and* extrinsic porosity within the same molecular solid—that is, pores which run both through and between the cage units. This requires the development of cage tectons that assemble in predictable ways, which necessitates, in turn, the chemical incorporation of structure-directing functionality within the cage modules.

RESULTS

In this study, we present two new cage molecules (**CC9** and **CC10**) with bulky aryl groups attached to the vertices (Figure 1). Our simple design premise was that these bulky directing groups might frustrate molecular packing and create additional extrinsic porosity between the cage units, thus enhancing the pore volume in comparison with our previous materials.[30] We also chose to investigate the effect of changing the functionalization on the aryl directing groups, and to explore whether this could be used to further vary the packing mode of the cages.

Cages **CC9** and **CC10** were synthesized by cycloimination of 1,3,5-triformylbenzene with (*R*,*R*)-1,2-diphenylethylenediamine and (*R*,*R*)-1,2-bis(4-fluorophenyl)ethane-1,2-diamine, respectively, in dichloromethane using trifluoroacetic acid as a catalyst (Figure 1). Under these reaction conditions, cage formation competes with a Diaza-Cope rearrangement of the same type used commonly to synthesize vicinal diamines.[39] As such, the production of the desired [4 + 6] imine cage is challenging, and indeed, a previous study reported that the (*R*,*R*)-1,2-diphenylethylenediamine cycloimination reaction does not occur.[40] The competing Diaza-Cope reaction requires a chair-shaped geometry to yield the undesirable rearranged side-product (Figure S1, Supporting Information (SI)). The key to producing these cages in viable yields was to slow down the rate of this rearrangement by cooling the reaction and, for **CC10**, to remove the condensation byproduct (water) using drying agents. A detailed account of the experimental methods is provided in the SI. After some optimization, **CC9** (1706 g mol^{-1}) and **CC10** (1922 g mol^{-1}) could be obtained in satisfactory yields of 35% and 37%, respectively, which is on a par with the initial, nonoptimized yields reported for our first generation of porous cage molecules.[30,35]

Mixing of a solution of **CC9** in dichloromethane with acetone—an antisolvent for **CC9**—causes precipitation of the solid cage in the trigonal space group *P*3 which is retained after full desolvation in vacuum. The desolvated structure was refined from powder X-ray diffraction data since no single crystals of sufficient quality could be obtained. Recrystallization from chloroform, and evaporation to

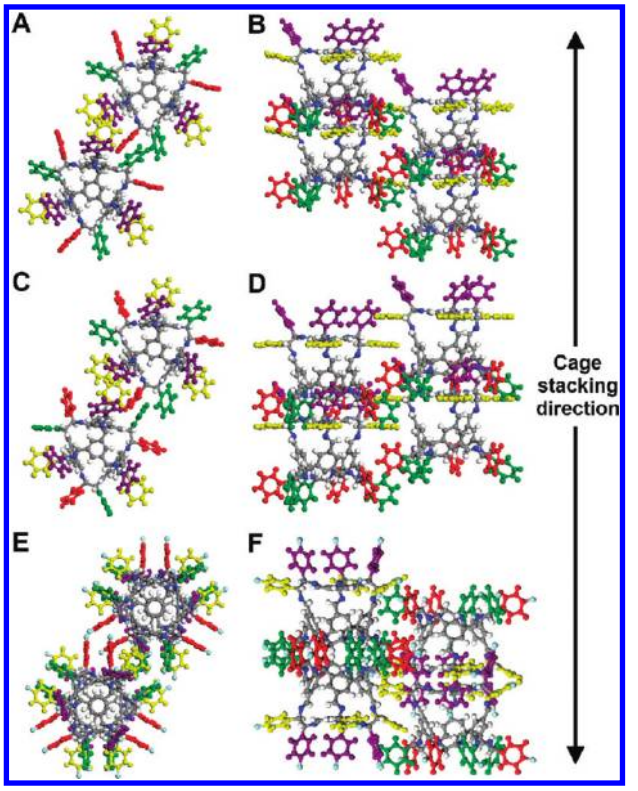

Figure 2. Solid-state packing for desolvated cages **CC9** (*R*3) (A, B), **CC9** (*P*3) (C, D), and **CC10** (E, F). Arenes with the same orientation with respect to the cage-core are color-coded to guide the eye.

dryness under nitrogen, yields a desolvated *R*3 polymorph of **CC9**. Single-crystal X-ray diffraction data refines to an almost fully desolvated structure with residual electron density attributed to 0.5 H_2O per cage molecule. Both polymorphs of **CC9** retain their long-range molecular order upon full desolvation. The single-crystal X-ray structure of the analogous fluorinated cage, **CC10**, refines as a solvate **CC10**·4.5$CHCl_3$·0.5H_2O in the space group *R*3 at 100 K. This material is readily desolvated, even by simple drying at ambient temperature, accompanied by a phase transition from *R*3 to *R*32. Heating the crystal to 350 K, followed by cooling under N_2 to ambient, gives a desolvated stoichiometry of **CC10**·0.5N_2 to account for residual electron density in the crystal. The desolvation process is accompanied by a reduction of scattering power due to the loss of heavy scatterers ($CHCl_3$) and, conceivably, some loss of order in the crystal.

The structures for in situ desolvated single crystals of **CC9** (*R*3) and **CC10** (*R*32), along with the refined structure obtained for a post-gas-sorption powder of **CC9** (*P*3), are shown in Figure 2. Each cage has four sets of three aryl groups related by three-fold symmetry; each set of three is shown in a different color in Figure 2. In both of the **CC9** polymorphs, neighboring cage molecules pack as 'stacks' in a window-to-face (AAAA) fashion, as indicated by the double-headed arrow in Figure 2. Adjacent 'stacks' are shifted along the *c*-axis with respect to each other and are symmetry-equivalent for the *R*3 polymorph, and independent for the *P*3 polymorph (Figure 2, B and D). In these stacks, one cage window is directed toward a neighboring arene face. The other three windows in both **CC9** (*R*3) and **CC9** (*P*3) point into two types of extrinsic pore void surrounding the cage stacks; one void is framed by the vicinal phenyl groups that are

oriented perpendicular to the *c*-axis (marked purple and yellow in Figure 2, A−D), and the other void is prescribed by phenyl groups that are oriented approximately parallel to the *c*-axis (red and green in Figure 2, A−D). The main difference between the two **CC9** polymorphs is a twist in the symmetry-equivalent phenyl groups, marked here in red and green, with respect to the principal crystallographic *c*-axis (Figure 2, A and C). For the *P*3 polymorph, this connects the intrinsic cage voids with the extrinsic pore space that is framed by the purple/yellow phenyl groups. This is apparent from the Connolly surface representations for the *R*3 and *P*3 polymorphs of **CC9**, as shown in Figure 3.

The fluorine-substituted analogue **CC10**, on the other hand, packs in an alternating window-to-window and face-to-face (ABAB) fashion (Figure 2, E and F). The reason for the difference in packing between **CC9** and **CC10** is not steric in nature because the spatial demands of the Ph- and F−Ar- groups are similar. Rather, the difference stems from heteroatomic and aromatic intermolecular interactions related to the fluorine functionalities in **CC10**.

A closer examination of the **CC10** structure reveals the presence of anisotropic electrostatic interactions. Neighboring molecules pack as face-to-face 'dimers' via the interdigitation of the 12 aryl groups on the cage faces—one such dimer interaction is illustrated in Figure 4A with the interdigitated aryl groups colored green and red. These aryl groups form alternating pairs showing either an aryl-to-aryl sandwich structure (marked red, Figure 4B) or a displaced stacking (marked green, Figure 4C). Both the sandwich structure and the displaced stacking arrangement have been predicted in other studies[41−43] to be attractive in nature using ab initio molecular mechanics and density functional calculations. The prime stabilization energy for the sandwich structure derives from London dispersion interactions, but this packing mode is deemed less favorable for most aromatic units because of resulting repulsion between π-electron clouds or between quadrupoles of equal sign.[42] The face-to-face sandwich

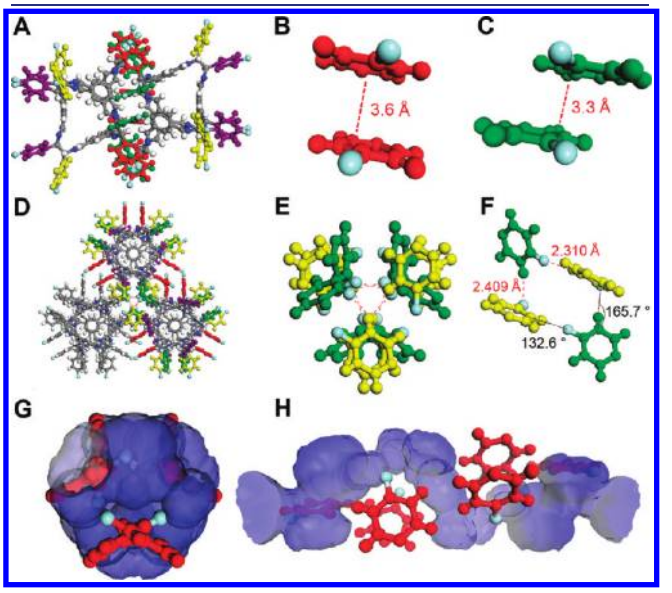

Figure 4. Scheme illustrating solid-state packing for **CC10**. Arenes with the same orientation with respect to the cage core are color-coded to guide the eye, as in Figure 2. In dimer shown (A), the red and green arenes interdigitate to form a mutual cage−cage void, connected by a window-to-window interaction but formally disconnected from the extrinsic, between-cage porosity and other cage−cage voids. C−H···F bonds are marked as dashed, red lines. Top-down (G) and perspective (H) views of the helical, 1-D extrinsic pore channel in **CC10**, spanned by vicinal aryl groups.

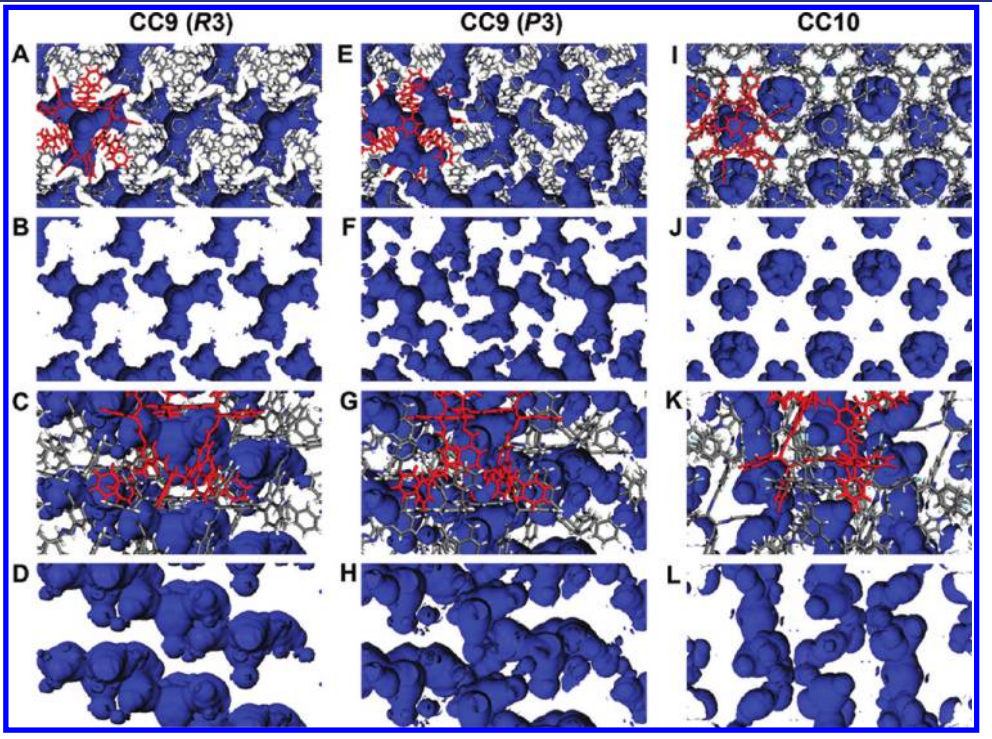

Figure 3. Connolly surface plots (blue) for **CC9** (*R*3) (A−D), **CC9** (*P*3) (E−H), and **CC10** (I−L) with a probe radius of 1.82 Å based on crystal structures for the desolvated materials shown along the *c*-axes with (A, E, I) and without (B, F, J) the cage framework, and along the *a*+*b* vector with (C, G, K) and without (D, H, L) the cage framework. These Connolly surfaces give an indication of pore connectivity; a single cage molecule (red) is highlighted in each of the overlay plots.

dx.doi.org/10.1021/ja2056374 |*J. Am. Chem. Soc.* 2011, 133, 16566–16571

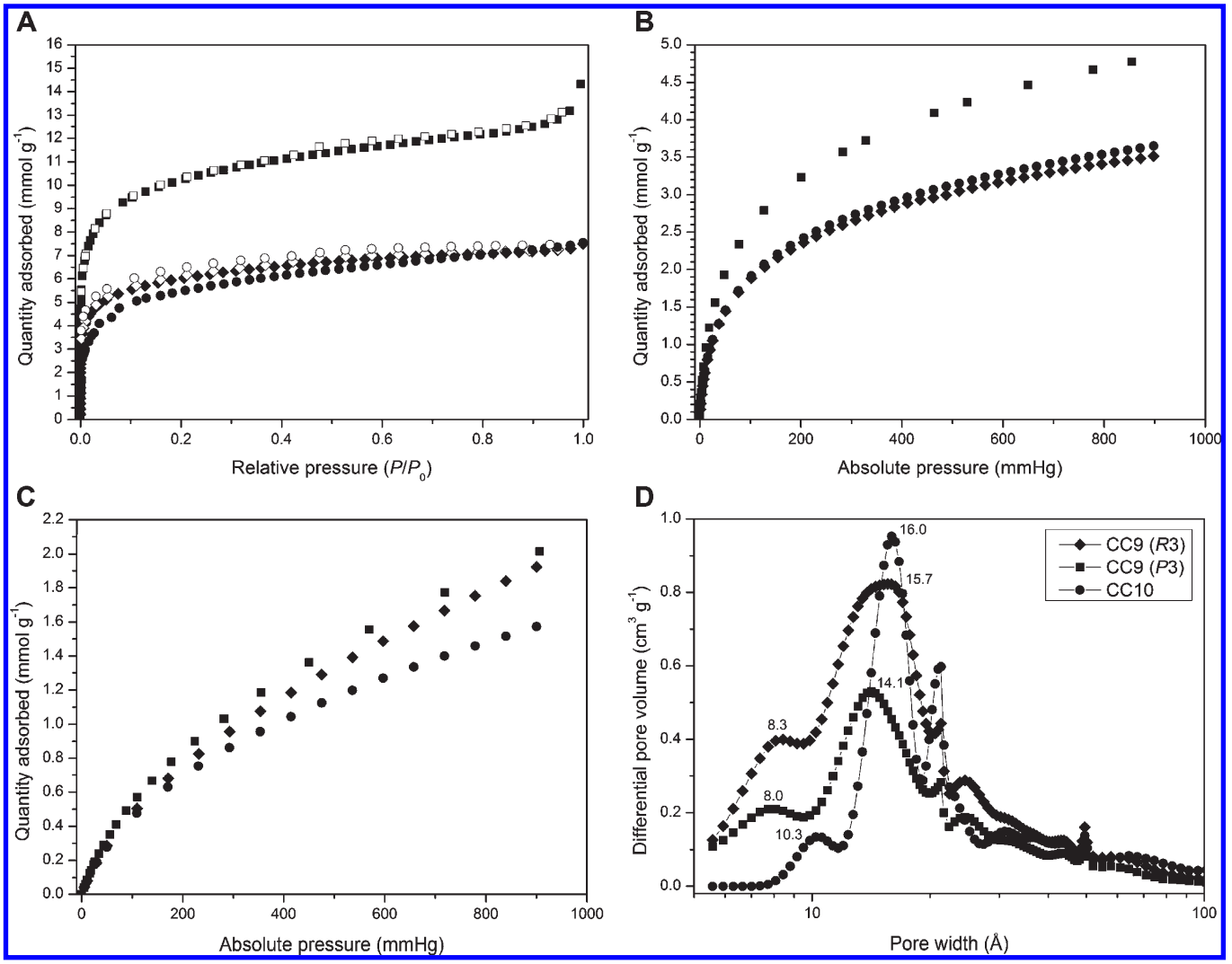

Figure 5. Nitrogen isotherms for **CC9** (*R*3) (◊), **CC9** (*P*3) (□), and **CC10** (○) (A). Filled and open symbols represent adsorption and desorption, respectively. Hydrogen adsorption isotherms (B) and carbon dioxide adsorption isotherms (C) for **CC9** (*R*3) (◊), **CC9** (*P*3) (□), and **CC10** (○). Nitrogen and hydrogen sorption isotherms were collected at 77 K; carbon dioxide adsorption isotherms at 273 K. The derived Langmuir surface area from the adsorption isotherm for **CC9** (*R*3), **CC9** (*P*3) and **CC10** is 575 $m^2 g^{-1}$ (SA_{BET} = 501 $m^2 g^{-1}$), 952 $m^2 g^{-1}$ (SA_{BET} = 854 $m^2 g^{-1}$) and 533 $m^2 g^{-1}$ (SA_{BET} = 460 $m^2 g^{-1}$), respectively. Comparison of micropore size distributions for **CC9** (*R*3) (◊), **CC9** (*P*3) (□), and **CC10** (○) as calculated using nonlocal density functional theory (D).

conformation (red aryl groups) shows a classical 3.6 Å separation, as observed for benzene and other aromatic, discotic systems.[44,45] Displaced stacking, as exhibited by the green aryl groups in Figure 4, has been ascribed to favorable alignment of the quadrupole moments in the aromatic units, which results in better stabilization.[46,47] The displaced aryl stacks in **CC10** have an interplanar distance of 3.3 Å and a lateral displacement of 2.1 Å, which is comparable with calculated values for gas- and liquid-phase orientation of aromatic units (3.4−3.6 Å and 1.6−1.8 Å for intermolecular distance and lateral displacement, respectively).[48,49] At the face-to-face intersection of neighboring **CC10** molecules, three aryl groups of each cage point almost perpendicular to the face-to-face plane, and these groups occlude the windows of adjacent cages (aryl groups colored purple in Figure 2F). As a consequence, each window-to-window molecular 'dimer' of **CC10** forms a mutual, conjoined cavity which is formally disconnected from the extrinsic void space between cages (Figure 3J).

■ DISCUSSION

The permanent porosity in these materials might be expected to depend on the level of connectivity between the intrinsic and extrinsic voids, and hence the accessibility of the two kinds of pore to guest molecules. Both desolvated polymorphs of **CC9** pack in a similar manner, forming cage 'stacks' parallel to the *c*-axis arranged in a pseudohexagonal fashion. Stacking is frustrated by the phenyl groups at the vertices. The extrinsic pore volume prescribed by the aryl groups is likewise arranged as a pseudohexagonal array of one-dimensional (1-D) channels along the *c*-axis. These 1-D channels are more interconnected with the intrinsic cage cavities for the *P*3 **CC9** polymorph, in comparison with *R*3 form, as a result of a relative twist in the phenyl vertex groups (Figure 3B and D).

Neither of the two polymorphs of **CC9** shows any significant close contacts shorter than 2.5 Å, as might be indicative of electrostatic interactions or hydrogen bonding. By contrast, the

dx.doi.org/10.1021/ja2056374 |*J. Am. Chem. Soc.* 2011, 133, 16566–16571

shape and nature of the extrinsic pore space in **CC10** is affected by anisotropic interactions. Inspection of close contacts below 2.5 Å reveals two different types of extrinsic pore spaces arranged in a pseudohexagonal fashion along the *c*-axis around a 'stack' of **CC10** dimers (Figures 4D and 3B). Unlike the 1-D channels in the **CC9** polymorphs, these extrinsic pore channels in **CC10** vary by the presence or absence of hydrogen bonds. For one of these extrinsic pore channels, aryl groups (colored green and yellow in Figure 4) from three neighboring cage stacks engage in a pattern of cooperative C−H···F bonds (Figure 4E and F). This pattern has been observed previously, and exclusively, for small organofluorines, and has been defined as a rare supramolecular synthon of fluorobenzene.[50,51] The two C−H···F bond lengths observed in **CC10** are 2.3 and 2.4 Å, with C−H···F angles of 132.6° and 165.7°, respectively (Figure 4F). These values match closely with those reported in the Cambridge Structure Database (CSD) for smaller molecules, as summarized by others.[52,53] This hydrogen-bonding pattern effectively 'seals' this set of extrinsic pore channels to guest molecules, as reflected in the Connolly surface plots for **CC10** (Figure 3). The other set of 1-D channels, by contrast, shows no sign of the influence of anisotropic electrostatic interactions. Here, the aryl units (marked red in Figure 4, G and H) are sufficiently far apart to give rise to a helical 1-D pore channel. Interestingly, for both hydrogen bonded and the aforementioned $\pi-\pi$ stacked aryls, the groups assume orientations close to or identical to the most favorable packing observed for smaller, 'free' molecular entities,[52,53] despite the fact that the vertex arenes in **CC10** are locked into place relative to one another by the cage core. It is anisotropic ordering which enforces the geometry of **CC10**, and this may also be the reason that polymorphism has not yet been observed for this cage.

The desolvated molecular solids for **CC9** (both polymorphs) and **CC10** adsorb large quantities of gases. The Langmuir surface areas calculated from the Type I nitrogen sorption isotherms were 952 $m^2\ g^{-1}$ (SA_{BET} = 854 $m^2\ g^{-1}$) for **CC9** (*P*3), 575 $m^2\ g^{-1}$ (SA_{BET} = 501 $m^2\ g^{-1}$) for **CC9** (*R*3), and 533 $m^2\ g^{-1}$ (SA_{BET} = 460 $m^2\ g^{-1}$) for **CC10** (Figure 5). Pore size distributions calculated by nonlocal density functional theory from the adsorption branches show two main peaks in the micropore region for each of these materials. The set of smaller pore sizes is comparable with the static diameters of the windows of individual cage molecules of approximately 6 Å. All materials were reanalyzed after gas-sorption analysis by powder X-ray diffraction, and the obtained data was refined against the crystal structures of the desolvated materials to ensure that no chemical decomposition or permanent structural rearrangement had accompanied the degassing or sorption processes. The nitrogen uptake at 77 K for both **CC9** (*R*3) and **CC10** amounts to 7.5 mmol g^{-1}, while the *P*3 polymorph of **CC9** adsorbs almost twice as much gas (14.3 mmol g^{-1}). Both of the CC9 polymorphs show classical Type I nitrogen sorption behavior, while the isotherm for **CC10** is hysteretic almost over the entire pressure range. Similarly, **CC9** (*R*3) and **CC10** absorb 3.5 mmol g^{-1} (0.70 wt %) and 3.6 mmol g^{-1} (0.73 wt %) of hydrogen at 77 K, while **CC9** (*P*3) shows a larger uptake of 4.8 mmol g^{-1} (0.96 wt %). At higher temperatures (273 K), the three cage structures adsorb more similar quantities of CO_2: 1.9 mmol g^{-1} for **CC9** (*R*3), 2.0 mmol g^{-1} for **CC9** (*P*3), and 1.6 mmol g^{-1} for **CC10**. To put these results into perspective, the crystalline porous solid **CC9** (*P*3) has a higher apparent surface area and adsorbs more N_2 than any of the comparably sized cages that we reported initially,[30] although it is surpassed by two larger cages reported recently, one by Mastalerz[32] and one by our own group.[33] As such, our strategy of producing additional, extrinsic pore volume via the introduction of bulkier vertices is successful, at least for **CC9** (*P*3), as evidenced both by crystallography and gas sorption analysis. It should be noted here that gas sorption in solids such as this cannot always be justified by crystal structures alone. For example, crystalline defects and surface barriers may influence sorption, and these are not captured by X-ray crystallography.[54,55] Moreover, any amorphized impurities, which might be 'invisible' to X-ray methods, could contribute to, rather than reduce, the pore volume in these solids.[56]

As outlined above, only a minor rotation of the relevant aryl groups about a C−C bond is 'gating' the pore connectivity between the intrinsic and extrinsic porosity in **CC9**. Thus, it is possible that low-energy cooperative dynamic processes may occur at more elevated temperatures involving transient rotation of these groups, perhaps explaining the smaller difference in CO_2 sorption observed between the two **CC9** polymorphs (Figure 5).[30,57]

CONCLUSIONS

To conclude, the vertex functionality in these new cages was chosen to enhance porosity with respect to our previous materials[30] by creating additional, extrinsic porosity to augment the intrinsic porosity within the cages. For the *P*3 polymorph of **CC9**, which can be crystallized reproducibly from chloroform, this strategy has succeeded. We have therefore demonstrated a pathway toward rational, synthetic design of additional extrinsic porosity within this class of intrinsically porous organic cage molecules. The vertex groups in **CC9** and **CC10** were chosen to direct molecular assembly in ways that are familiar in the fields of crystal engineering and supramolecular chemistry. The porous molecular crystals obtained show exceptionally high gas uptakes within this class of material resulting from a combination of intrinsic and extrinsic pore volumes. These observations raise the question of how we might enhance porosity further in such materials. One design principle would be to develop cage tectons that show anisotropic ordering to minimize the potential surface area in each molecule that is lost in the form of intermolecular contacts. That is, we propose to search for tectons that form porous solids comprising, as nearly as possible, 'point contacts' between molecules such that the guest-accessible surface is maximized. In this respect, hydrogen bonding at 'sticky' functionalized vertices is a promising tool.[58] Such concepts are supported by this study which shows that the introduction of more robust intermolecular bonding interactions can modulate the diffusion of gas molecules through porous molecular solids. This could be relevant for tunable molecular separations or for trapping specific guests.

ASSOCIATED CONTENT

Supporting Information. Materials and synthetic procedures, analytical methods, nuclear magnetic resonance spectra (NMR), matrix-assisted laser desorption/ionization time-of-flight mass spectra (MALDI-TOF), scanning electron microscopy (SEM), single and powder X-ray diffraction analysis, gas sorption analysis, and all references including the complete reference for ref 30. This material is available free of charge via the Internet at http://pubs.acs.org.

AUTHOR INFORMATION

Corresponding Author
aicooper@liv.ac.uk

ACKNOWLEDGMENT

We thank the Engineering and Research Council (EPSRC) for financial support under Grant EP/H000925/1. A.I.C. is a Royal Society Wolfson Research Merit Award holder. We thank the STFC for access to Diamond Light Source and the staff at beamline I11.

REFERENCES

(1) Wright, P. A. *Microporous Framework Solids*; Royal Society of Chemistry: Cambridge, UK, 2008.
(2) Yaghi, O. M.; O'Keeffe, M.; Ockwig, N. W.; Chae, H. K.; Eddaoudi, M.; Kim, J. *Nature* **2003**, *423*, 705.
(3) Zhao, X. B.; Xiao, B.; Fletcher, A. J.; Thomas, K. M.; Bradshaw, D.; Rosseinsky, M. J. *Science* **2004**, *306*, 1012.
(4) Lee, J.; Farha, O. K.; Roberts, J.; Scheidt, K. A.; Nguyen, S. T.; Hupp, J. T. *Chem. Soc. Rev.* **2009**, *38*, 1450.
(5) Horike, S.; Shimomura, S.; Kitagawa, S. *Nature Chem.* **2009**, *1*, 695.
(6) Budd, P. M.; Ghanem, B. S.; Makhseed, S.; McKeown, N. B.; Msayib, K. J.; Tattershall, C. E. *Chem. Commun.* **2004**, 230.
(7) Jiang, J. X.; Su, F.; Trewin, A.; Wood, C. D.; Campbell, N. L.; Niu, H.; Dickinson, C.; Ganin, A. Y.; Rosseinsky, M. J.; Khimyak, Y. Z.; Cooper, A. I. *Angew. Chem., Int. Ed.* **2007**, *46*, 8574.
(8) Weber, J.; Antonietti, M.; Thomas, A. *Macromolecules* **2007**, *40*, 1299.
(9) Ben, T.; Ren, H.; Ma, S. Q.; Cao, D. P.; Lan, J. H.; Jing, X. F.; Wang, W. C.; Xu, J.; Deng, F.; Simmons, J. M.; Qiu, S. L.; Zhu, G. S. *Angew. Chem., Int. Ed.* **2009**, *48*, 9457.
(10) McKeown, N. B.; Budd, P. M. *Macromolecules* **2010**, *43*, 5163.
(11) Schmidt, J.; Werner, M.; Thomas, A. *Macromolecules* **2009**, *42*, 4426.
(12) Côté, A. P.; Benin, A. I.; Ockwig, N. W.; O'Keeffe, M.; Matzger, A. J.; Yaghi, O. M. *Science* **2005**, *310*, 1166.
(13) Uribe-Romo, F. J.; Hunt, J. R.; Furukawa, H.; Klock, C.; O'Keeffe, M.; Yaghi, O. M. *J. Am. Chem. Soc.* **2009**, *131*, 4570.
(14) Dawson, R.; Laybourn, A.; Clowes, R.; Khimyak, Y. Z.; Adams, D. J.; Cooper, A. I. *Macromolecules* **2009**, *42*, 8809.
(15) Yaghi, O. M.; Li, H. L.; Davis, C.; Richardson, D.; Groy, T. L. *Acc. Chem. Res.* **1998**, *31*, 474.
(16) Olson, D. A.; Chen, L.; Hillmyer, M. A. *Chem. Mater.* **2008**, *20*, 869.
(17) Thomas, A.; Goettmann, F.; Antonietti, M. *Chem. Mater.* **2008**, *20*, 738.
(18) Thomas, A. *Angew. Chem., Int. Ed.* **2010**, *49*, 8328.
(19) Holst, J. R.; Trewin, A.; Cooper, A. I. *Nature Chem.* **2010**, *2*, 915.
(20) McKeown, N. B. *J. Mater. Chem.* **2010**, *20*, 10588.
(21) Atwood, J. L.; Barbour, L. J.; Jerga, A. *Science* **2002**, *296*, 2367.
(22) Udachin, K. A.; Moudrakovski, I. L.; Enright, G. D.; Ratcliffe, C. I.; Ripmeester, J. A. *Phys. Chem. Chem. Phys.* **2008**, *10*, 4636.
(23) Cram, D. J. *Science* **1983**, *219*, 1177.
(24) Collet, A. *Tetrahedron* **1987**, *43*, 5725.
(25) Hof, F.; Craig, S. L.; Nuckolls, C.; Rebek, J. *Angew. Chem., Int. Ed.* **2002**, *41*, 1488.
(26) Leontiev, A. V.; Rudkevich, D. M. *Chem. Commun.* **2004**, 1468.
(27) Inokuma, Y.; Arai, T.; Fujita, M. *Nature Chem.* **2010**, *2*, 780.
(28) Tranchemontagne, D. J. L.; Ni, Z.; O'Keeffe, M.; Yaghi, O. M. *Angew. Chem., Int. Ed.* **2008**, *47*, 5136.
(29) Mastalerz, M. *Angew. Chem., Int. Ed.* **2010**, *49*, 5042.
(30) Tozawa, T.; et al. *Nat. Mater.* **2009**, *8*, 973.
(31) Jones, J. T. A.; Holden, D.; Mitra, T.; Hasell, T.; Adams, D. J.; Jelfs, K. E.; Trewin, A.; Willock, D. J.; Day, G. M.; Bacsa, J.; Steiner, A.; Cooper, A. I. *Angew. Chem., Int. Ed.* **2011**, *50*, 749.
(32) Mastalerz, M.; Schneider, M. W.; Oppel, I. M.; Presly, O. *Angew. Chem., Int. Ed.* **2011**, *50*, 1046.
(33) Jones, J. T. A.; Hasell, T.; Wu, X. F.; Bacsa, J.; Jelfs, K. E.; Schmidtmann, M.; Chong, S. Y.; Adams, D. J.; Trewin, A.; Schiffman, F.; Cora, F.; Slater, B.; Steiner, A.; Day, G. M.; Cooper, A. I. *Nature* **2011**, *474*, 367.
(34) Cooper, A. I. *Angew. Chem., Int. Ed.* **2011**, *50*, 996.
(35) Lydon, D. P.; Campbell, N. L.; Adams, D. J.; Cooper, A. I. *Synth. Commun.* **2011**, *41*, 2146.
(36) Price, S. L. *Acc. Chem. Res.* **2009**, *42*, 117.
(37) Eddaoudi, M.; Kim, J.; Rosi, N.; Vodak, D.; Wachter, J.; O'Keeffe, M.; Yaghi, O. M. *Science* **2002**, *295*, 469.
(38) Desiraju, G. R. *Angew. Chem., Int. Ed.* **1995**, *34*, 2311.
(39) Kim, H.; Staikova, M.; Lough, A. J.; Chin, J. *Org. Lett.* **2009**, *11*, 157.
(40) Skowronek, P.; Gawronski, J. *Org. Lett.* **2008**, *10*, 4755.
(41) Meyer, E. A.; Castellano, R. K.; Diederich, F. *Angew. Chem., Int. Ed.* **2003**, *42*, 1210.
(42) Smith, G. D.; Jaffe, R. L. *J. Phys. Chem.* **1996**, *100*, 9624.
(43) Tsuzuki, S.; Honda, K.; Uchimaru, T.; Mikami, M.; Tanabe, K. *J. Am. Chem. Soc.* **2001**, *124*, 104.
(44) Gervasio, F. L.; Chelli, R.; Procacci, P.; Schettino, V. *J. Phys. Chem. A* **2002**, *106*, 2945.
(45) Sinnokrot, M. O.; Valeev, E. F.; Sherrill, C. D. *J. Am. Chem. Soc.* **2002**, *124*, 10887.
(46) Dennis, G. R.; Ritchie, G. L. D. *J. Phys. Chem.* **1991**, *95*, 656.
(47) Blanchard, M. D.; Hughes, R. P.; Concolino, T. E.; Rheingold, A. L. *Chem. Mater.* **2000**, *12*, 1604.
(48) Gonzalez, C.; Lim, E. C. *J. Phys. Chem. A* **2000**, *104*, 2953.
(49) Lee, N. K.; Park, S.; Kim, S. K. *J. Chem. Phys.* **2002**, *116*, 7910.
(50) Thalladi, V. R.; Weiss, H.-C.; Bläser, D.; Boese, R.; Nangia, A.; Desiraju, G. R. *J. Am. Chem. Soc.* **1998**, *120*, 8702.
(51) Dunitz, J. D.; Taylor, R. *Chem.—Eur. J.* **1997**, *3*, 89.
(52) D'Oria, E.; Novoa, J. J. *CrystEngComm* **2008**, *10*, 423.
(53) Merz, K.; Vasylyeva, V. *CrystEngComm* **2010**, *12*, 3989.
(54) Sholl, D. S. *Nature Chem.* **2011**, *3*, 429.
(55) Hibbe, F.; Chmelik, C.; Heinke, L.; Pramanik, S.; Li, J.; Ruthven, D. M.; Tzoulaki, D.; Kärger, J. R. *J. Am. Chem. Soc.* **2011**, *133*, 2804.
(56) Jiang, S.; Jones, J. T. A.; Hasell, T.; Blythe, C. E.; Adams, D. J.; Trewin, A.; Cooper, A. I. *Nat. Commun.* **2011**, *2*, 207.
(57) Atwood, J. L.; Barbour, L. J.; Jerga, A.; Schottel, B. L. *Science* **2002**, *298*, 1000.
(58) Wuest, J. D. *Chem. Commun.* **2005**, 5830.